Rajabi, M., Ziegler, M., Tingay, M., Heidbach, O., Reynolds, S. (2016): Contemporary tectonic stress pattern of the Taranaki Basin, New Zealand. - *Journal of Geophysical Research*, *121*, 8, pp. 6053—6070.

DOI: http://doi.org/10.1002/2016JB013178

AGU PUBLICATIONS

JGR

Journal of Geophysical Research: Solid Earth

RESEARCH ARTICLE
10.1002/2016JB013178

Key Points:
- The first detailed wellbore-derived basin-scale in situ stress analysis in New Zealand
- Interpretation and analysis of present-day stress in the Taranaki Basin with 198 data records
- Slab geometry and associated forces are the key control of crustal stress in the Taranaki Basin

Supporting Information:
- Supporting Information S1

Correspondence to:
M. Rajabi,
mojtaba.rajabi@adelaide.edu.au

Citation:
Rajabi, M., M. Ziegler, M. Tingay, O. Heidbach, and S. Reynolds (2016), Contemporary tectonic stress pattern of the Taranaki Basin, New Zealand, *J. Geophys. Res. Solid Earth*, *121*, 6053–6070, doi:10.1002/2016JB013178.

Received 16 MAY 2016
Accepted 11 JUL 2016
Accepted article online 13 JUL 2016
Published online 3 AUG 2016

Contemporary tectonic stress pattern of the Taranaki Basin, New Zealand

Mojtaba Rajabi[1], Moritz Ziegler[2,3], Mark Tingay[1], Oliver Heidbach[2], and Scott Reynolds[4]

[1]Australian School of Petroleum, University of Adelaide, Adelaide, South Australia, Australia, [2]Helmholtz Centre Potsdam, German Research Centre for Geosciences GFZ, Potsdam, Germany, [3]Institute of Earth and Environmental Science, University of Potsdam, Potsdam, Germany, [4]Ikon Science Asia Pacific, Kuala Lumpur, Malaysia

Abstract The present-day stress state is a key parameter in numerous geoscientific research fields including geodynamics, seismic hazard assessment, and geomechanics of georeservoirs. The Taranaki Basin of New Zealand is located on the Australian Plate and forms the western boundary of tectonic deformation due to Pacific Plate subduction along the Hikurangi margin. This paper presents the first comprehensive wellbore-derived basin-scale in situ stress analysis in New Zealand. We analyze borehole image and oriented caliper data from 129 petroleum wells in the Taranaki Basin to interpret the shape of boreholes and determine the orientation of maximum horizontal stress (S_{Hmax}). We combine these data (151 S_{Hmax} data records) with 40 stress data records derived from individual earthquake focal mechanism solutions, 6 from stress inversions of focal mechanisms, and 1 data record using the average of several focal mechanism solutions. The resulting data set has 198 data records for the Taranaki Basin and suggests a regional S_{Hmax} orientation of N068°E (±22°), which is in agreement with NW-SE extension suggested by geological data. Furthermore, this ENE-WSW average S_{Hmax} orientation is subparallel to the subduction trench and strike of the subducting slab (N50°E) beneath the central western North Island. Hence, we suggest that the slab geometry and the associated forces due to slab rollback are the key control of crustal stress in the Taranaki Basin. In addition, we find stress perturbations with depth in the vicinity of faults in some of the studied wells, which highlight the impact of local stress sources on the present-day stress rotation.

1. Introduction

Subduction zones and their associated forces are supposed to provide the first-order control, amongst other plate boundary forces, on the regional pattern of crustal stress in intraplate and near-plate boundary zones [*Coblentz et al*., 1998; *Heidbach et al*., 2010; *Lithgow-Bertelloni and Guynn*, 2004; *Tingay et al*., 2010; *Zoback*, 1992; *Zoback et al*., 1989]. However, there are several mechanisms and features associated with subduction that affect the neotectonic activity of adjacent plates and generate complex stress patterns, particularly in the overriding plate [*Heidbach et al*., 2010; *Lallemand et al*., 2005; *Zoback*, 1992]. Understanding of these mechanisms, and their roles on the present-day stress pattern, has numerous applications in Earth sciences, including geodynamics, neotectonic deformation, seismic hazard assessment, mitigating induced seismicity, and enhancing production from hydrocarbon reservoirs [*Bell*, 1996b; *Engelder*, 1993; *Richardson*, 1992; *Sibson et al*., 2012; *Zoback*, 2007].

The Taranaki Basin of New Zealand is located ~400 km west of the Hikurangi margin, where the oblique subduction of the Pacific Plate actively occurs (west southwestward) beneath the (Indo-) Australian Plate (Figure 1) [*Beavan et al*., 2002; *DeMets et al*., 2010]. The basin originally formed in the Late Cretaceous as a rifted basin due to the Gondwana breakup and is now considered to mark the western limit of tectonic deformation related to the Hikurangi subduction zone [*Giba et al*., 2010; *King and Thrasher*, 1996; *Reilly et al*., 2015]. The Taranaki Basin has had a complex structural and geological history, right from its earliest initiation up until the present day, and currently displays active tectonics, volcanism, and seismicity [*Anderson and Webb*, 1994; *Giba et al*., 2010; *Neall et al*., 1986; *Robinson et al*., 1976; *Sherburn and White*, 2005; 2006]. The complex geological and structural history of the Taranaki Basin makes it ideally prospective for hydrocarbons, as it contains all the required elements of a commercial petroleum system [*King and Thrasher*, 1996; *Stagpoole and Funnell*, 2001]. Indeed, the Taranaki Basin is the only petroleum-producing basin in New Zealand, with over 400 onshore and offshore drilled wells [*King and Thrasher*, 1996].

Despite the considerable level of interest in neotectonic deformation and seismic hazard assessment in New Zealand, as well as the economic importance of the Taranaki Basin, there are surprisingly few in situ stress

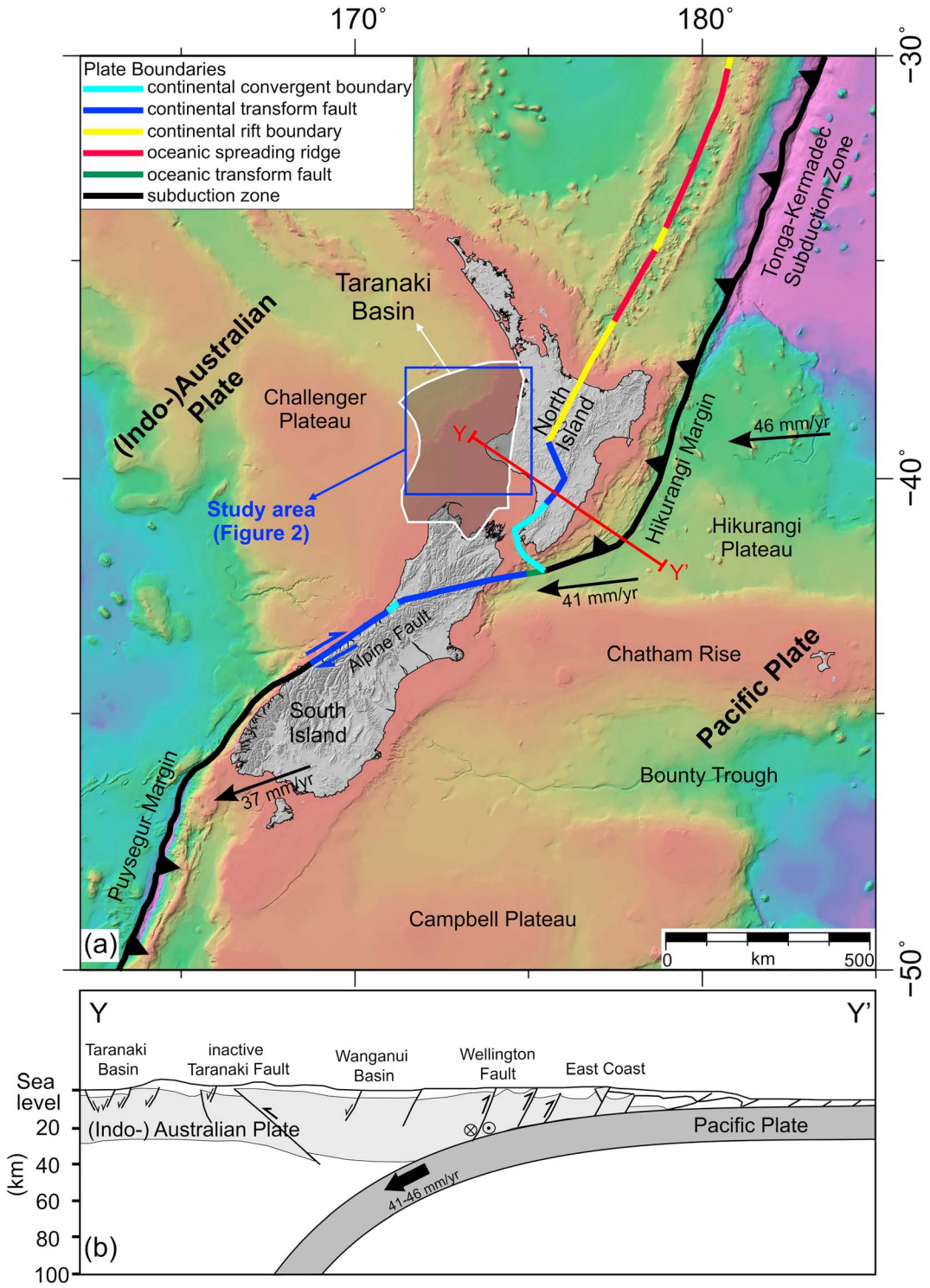

Figure 1. (a) Simplified tectonic setting of New Zealand which is located at the boundary of Pacific and (Indo-) Australian Plate (IAP). Pacific Plate Subduction beneath the IAP is the key control of the tectonic setting of overriding plate. In the south, the IAP is subducting beneath the Pacific Plate along Puysgur Margin. These two large subduction zones are linked to each other by the strike-slip Alpine Fault. The tectonic plate boundaries and their types are from *Bird* [2003]. The Taranaki Basin in western North Island is considered as the western limit of deformation due to subduction zone [*Giba et al.*, 2010; *Nicol and Wallace*, 2007; *Sherburn and White*, 2006]. (b) Regional cross section across North Island and the Taranaki Basin that show the position of subduction along the Hikurangi margin [*Giba et al.*, 2010].

data in the published literature for the region. For example, the 2008 release of the World Stress Map (WSM) database, which is the most comprehensive worldwide compilation of the stress data, contains no stress information at all in and around the Taranaki Basin [*Heidbach et al*., 2008; 2010]. The only published study the authors could find on the in situ stress of the Taranaki Basin was carried out by *Sherburn and White* [2006], which was based on 39 individual focal mechanism solutions (FMS) and two formal inversion of earthquake focal mechanisms (FMF) of deep (>7.5 km) earthquakes, and suggested an E-W orientation of the maximum horizontal stress (S_{Hmax}). In addition, *Townend et al*. [2012] published the most comprehensive stress map of New Zealand and also suggested an E-W S_{Hmax} orientation for the region based on four FMF data records and the results of *Sherburn and White* [2006].

Borehole imaging technology and oriented caliper data provide information on the shape of borehole wall and are well established methods for determination of the present-day S_{Hmax} orientation [*Bell*, 1996a; *Zoback*, 2007]. In this study we compile and interpret different types of borehole image log, Schlumberger's high-resolution dipmeter tool, and oriented caliper data from 129 wells to determine the orientation of the S_{Hmax} across the Taranaki Basin. We also compile FMS and FMF data of earthquakes from the published literature to present the first comprehensive stress map of the Taranaki Basin. We use two common circular statistical methods to analyze the regional pattern of S_{Hmax} and compare the present-day stress pattern with different geological information in and around the Taranaki Basin. On a large scale, we compare the S_{Hmax} pattern with the geometry of the Hikurangi margin subduction zone east of the basin and propose that subduction processes control the stress pattern of the Taranaki Basin at the first order. On smaller scales, we highlight some local stress perturbations in the vicinity of faults and describe the significant implications of both the regional and highly localized, stress orientations for petroleum exploration and production in the Taranaki Basin.

2. Tectonic and Geological Setting of the Taranaki Basin

The mostly offshore and partly onshore Taranaki Basin is located on the western side of New Zealand's North Island and covers an area of 330,000 km^2 (Figure 1) [*Salazar et al*., 2015]. The basin has a complex tectonic history, including two major phases of extension and one of compression since the Late Cretaceous [*Giba et al*., 2010; *King and Thrasher*, 1996; *Nicol et al*., 2005; *Reilly et al*., 2015]. During the Late Cretaceous-late Paleocene, the Taranaki Basin was initiated as an intracontinental rifted basin due to the breakup of eastern Gondwana and the opening of the Tasman Sea [*Giba et al*., 2010; *King and Thrasher*, 1996]. This first phase of extension was followed by an Eocene (or Oligocene) and younger phase of compression and then by a second NW-SE extensional phase that has been ongoing from the Plio-Pleistocene (or late Miocene) to present day [*Giba et al*., 2010; *Holt and Stern*, 1994; *King and Thrasher*, 1996; *Nicol et al*., 2005; *Reilly et al*., 2015; *Stern and Davey*, 1990]. Synchronous extension and shortening at the present day occurs in the north and south of the Taranaki Basin, respectively, due to clockwise block rotation around a southward migrating vertical axis [*Giba et al*., 2010; *King and Thrasher*, 1996; *Reilly et al*., 2015]. The Taranaki Basin is now considered an active marginal basin and forms the western limit of tectonic deformation related to Pacific Plate subduction beneath the Australian Plate along the Hikurangi margin (Figures 1 and 2) [*Hill et al*., 2004; *King and Thrasher*, 1996; *Palmer and Bulte*, 1991; *Stagpoole and Funnell*, 2001; *Stagpoole et al*., 2004; *Webster et al*., 2011].

The present-day Taranaki Basin is characterized by two structural blocks, termed the western stable platform (passive margin) and eastern mobile belt (active margin) (Figure 2) [*King and Thrasher*, 1996]. The western stable platform is relatively undeformed, while the active part of the basin (i.e., eastern mobile belt) is characterized by a variety of different structures, including thrust and overthrust features, inversion structures, extensional features, and a belt of stratovolcanoes [*Giba et al*., 2010; *King and Thrasher*, 1996; *Reilly et al*., 2015]. The Taranaki Fault and the Cape Egmont Fault Zone (CEFZ), respectively, define the eastern and western boundaries of the eastern mobile belt that has accommodated the thick sedimentary sequences and petroleum plays of the Taranaki Basin (Figure 2) [*King and Thrasher*, 1996; *Muir et al*., 2000]. The CEFZ is a group of extensional and compressional active faults with a regional NE-SW orientation. However, the N-S striking Taranaki Fault is a major Tertiary structure that forms the boundary of Mesozoic basement and Cretaceous-Tertiary rocks and has regionally accommodated much of the large-scale plate convergence displacement (Figure 2) [*Nicol et al*., 2004; *Stagpoole et al*., 2004].

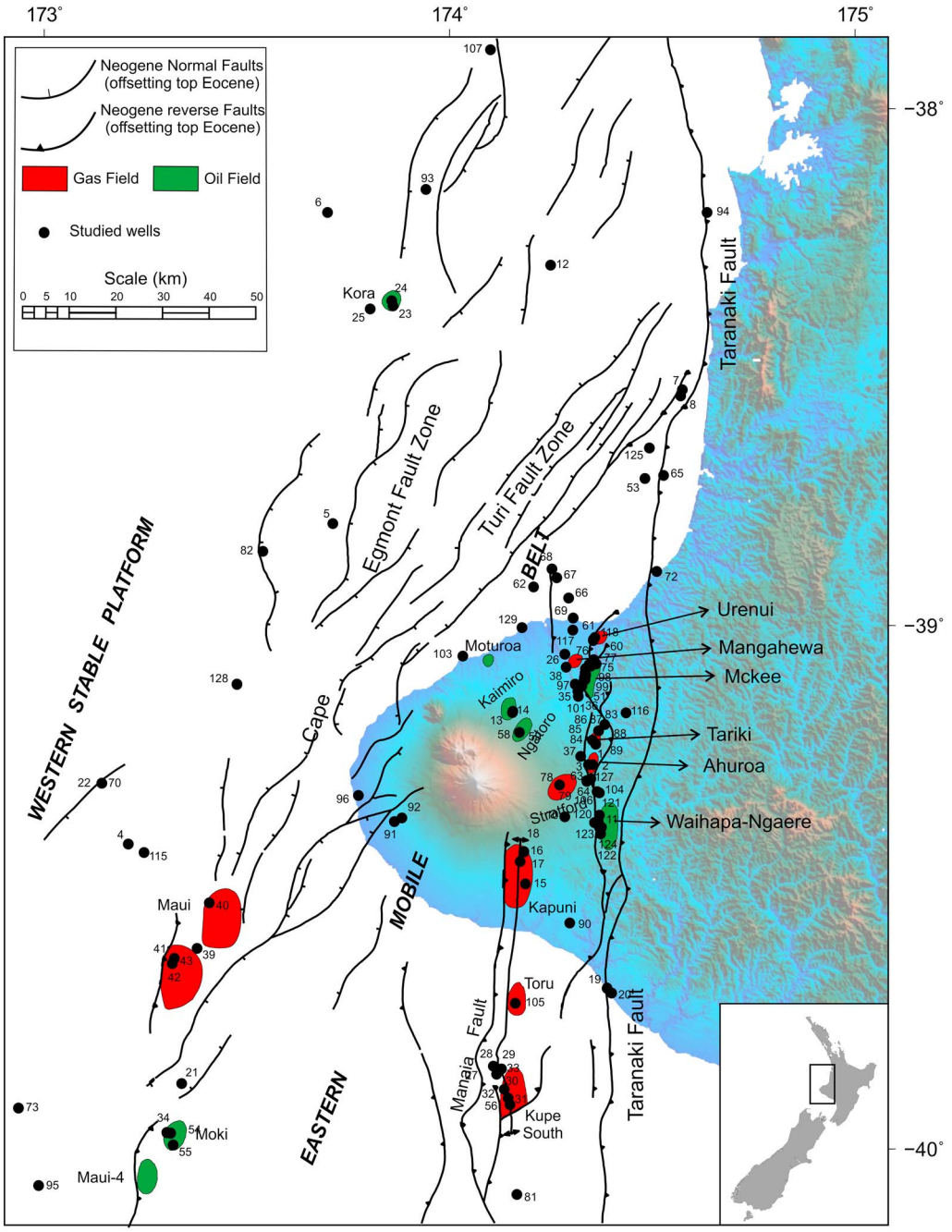

1:Ahuroa-1	20:Kauri-A1	39:Maui-5	58:Ngatoro-1	77:Pukemai-3	96:Tipoka-1	115:Tui-1
2:Ahuroa-1A	21:Kea-1	40:Maui-6	59:Ngatoro-6	78:Stratford-1	97:Toetoe-1	116:Tuihu-1
3:Ahuroa-2A	22:Kopuwai-1	41:Maui-7	60:Ohanga-1	79:Stratford-1A	98:Toetoe-2C	117:Turangi-1
4:Amokura-1	23:Kora-1	42:MB-P(8)	61:Ohanga-2	80:Surville-1	99:Toetoe-3	118:Urenui-1
5:Arawa-1	24:Kora-3	43:MB-V(3)	62:Okoki-1	81:Tahi-1	100:Toetoe-3A	119:Waihapa-1A
6:Ariki-1	25:Kora-4	44:McKee-1	63:Piakau North-A1	82:Taimana-1	101:Toetoe-4	120:Waihapa-2
7:Awakino South-1	26:Kowhai-A1	45:McKee-2	64:Piakau-1	83:Tariki North-1A	102:Toetoe-7	121:Waihapa-4
8:Awakino-1	27:Kupe South-1	46:McKee-3	65:Pluto-1	84:Tariki-1	103:Toka-1	122:Waihapa-5
9:Cape Farewell-1	28:Kupe South-2	47:McKee-3a	66:Pohokura-1	85:Tariki-1A	104:Toko-1	123:Waihapa-6
10:Cardiff-1	29:Kupe South-3B	48:McKee-4	67:Pohokura-2	86:Tariki-2	105:Toru-1	124:Waihapa-6A
11:Goss-A1	30:Kupe South-4	49:McKee-5	68:Pohokura-3	87:Tariki-2A	106:Trapper A-1	125:Waihi-1
12:Kahawai-1	31:Kupe South-5	50:McKee-5A	69:Pohokura South-1	88:Tariki-2B	107:Tua Tua-1	126:Waitui
13:Kaimiro-1	32:Kupe South-6	51:McKee-6/6A	70:Pohutukawa A-1	89:Tariki-3	108:Tuhua-1	127:Wharehuia-1
14:Kaimiro-2-ST1	33:Kupe South-7ST1	52:McKee-7/7A	71:Pouri-1	90:Tawa-B1	109:Tuhua-2	128:Witiora-1
15:Kapuni 17	34:Maari-1	53:Mokau-1	72:Pukearuhe-1	91:Te Kiri-2	110:Tuhua-2A	129:Waimanu-1
16:Kapuni-12	35:Makara-1	54:Moki-1	73:Pukeko-1	92:Te Kiri-1	111:Tuhua-2B	
17:Kapuni-14	36:Makara-1B	55:Moki-2A	74:Pukemai-1	93:Te Kumi-1	112:Tuhua-3	
18:Kapuni-15	37:Makuri-1A	56:Momoho-1	75:Pukemai-2	94:Te Ranga-1	113:Tuhua-4	
19:Kauri-E11	38:Mangahewa-04	57:Motueka-1	76:Pukemai-2A	95:Te Whatu-2	114:Tuhua-5	

Figure 2. Structural elements of the Taranaki Basin and location of the studied wells. Western Stable Platform and Eastern Mobile Belt are two major structural blocks [*King and Thrasher*, 1996]. Faults and the location of different oil and gas fields across the basin are from *King and Thrasher* [1996]. Detailed location of the studied wells can be found in the supporting information.

The Taranaki Basin is considered as a marine basin that is floored by extended continental crust and accommodates thick sequences of Cretaceous and younger sedimentary rocks in several depocenters [*King and Thrasher*, 1996]. The complex history of the Taranaki Basin provided all elements of petroleum systems for generation and accumulation of hydrocarbons in several trap types (Figure 2) [*King and Thrasher*, 1996]. Late Cretaceous to Paleogene coals and mudstones are the primary source rocks, while Paleocene to Pliocene sandstone formations are the principal reservoir rocks of the basin. Different mudstone and marly units (Late Cretaceous to Neogene) are the major top seals, with hydrocarbons trapped by faults, folds, and stratigraphic features across the basin [*King and Thrasher*, 1996].

3. Methods to Determine the Present-Day Stress Orientation

The in situ stress tensor is described with a symmetric second-degree tensor and thus consists of six independent components [*Engelder*, 1993; *Jaeger et al*., 2007; *Zoback*, 2007]. Assuming that the overburden stress (S_v) is one of the three principal stresses, the stress tensor in the Earth's crust can be explained by four independent components, termed the S_v magnitude, maximum horizontal stress (S_{Hmax}) magnitude, minimum horizontal stress (S_{hmin}) magnitude, and the S_{Hmax} orientation [*Bell*, 1996a; *Engelder*, 1993; *Jaeger et al*., 2007; *Zoback*, 2007]. Of all the components of the present-day stress tensor, the orientation of S_{Hmax} has received significant attention in the past 30 years due to its important implications for a wide variety of Earth science and engineering issues [*Bell*, 1996b; *Engelder*, 1993; *Heidbach et al*., 2010; *Tingay et al*., 2005; *Zoback*, 2007]. Herein we determined the orientation of the S_{Hmax} in vertical sections of the studied wells based on the WSM guidelines and criteria [*Heidbach et al*., 2010; *Sperner et al*., 2003; *Zoback*, 1992]. Wherever possible, we also determined the relative magnitude of the principal stresses, to define the tectonic stress regime based on the standard *Anderson* [1905] classification. In this study, we investigated the present-day state of crustal stress (from 0 to 40 km depth), and particularly the S_{Hmax} orientation, in the Taranaki Basin from four well-known methods, namely, borehole breakouts, drilling-induced fractures (DIFs), formal stress inversions of focal mechanisms (FMF), and focal mechanism solutions of earthquakes (FMS).

3.1. Determination of the S_{Hmax} Orientation From Drilling-Induced Fractures and Borehole Breakouts

The analyses of borehole breakouts and DIFs are well-known methods for interpretation of horizontal in situ stress orientations in boreholes [*Bell*, 1996a; *Zoback*, 2007; *Zoback et al*., 1989]. Borehole breakouts form where the hoop stress acting on the wellbore wall exceeds the compressive strength of rock and causes shear failure and spalling off of the rocks forming the wellbore wall [*Bell and Gough*, 1979]. In a vertical wellbore, borehole breakouts cause an enlargement of the hole diameter in the S_{hmin} orientation, which gives the borehole cross section an approximately oval shape, with the long axis of the ellipse aligned parallel to S_{hmin} [*Bell and Gough*, 1979]. The orientation of borehole breakouts, and thus the orientation of present-day S_{Hmax}, can be interpreted from borehole image logs and oriented four-arm or six-arm caliper logs [*Bell*, 1996a; *Plumb and Hickman*, 1985; *Zoback*, 2007].

It should be noted that borehole breakouts can be difficult to interpret from oriented caliper logs, as they need to be carefully distinguished from other types of non-stress-related borehole enlargements, such as key seats and washouts [*Plumb and Hickman*, 1985]. In this study, we used the commonly made assumption that one of the principal stresses is vertical. Therefore, in order to interpret the breakouts from caliper logs, wells with deviations $<10°$ were used. In wells with deviations $>5°$, breakouts were ignored if they coincided with the deviation direction, in order to filter out potential key seating. Hence, in this study we used the standard methodology introduced by *Plumb and Hickman* [1985] and *Bell* [1990], and expanded by *Reinecker et al*. [2003], to interpreted breakouts in the studied wells (Figure 3). Borehole image logs produce a 360° covered image of wellbore wall based on petrophysical property contrasts (e.g., resistivity or acoustic properties) and provide a more reliable interpretation of breakouts. In borehole image logs, breakouts are observed as relatively wide, "blobby" (often poorly resolved) zones of either high conductivity (in electrical image logs) or low-amplitude/high borehole radius (in acoustic image logs) appearing on opposite sides of the wellbore wall (Figure 3).

DIFs are created when the minimum principal effective stress, in the disturbed stress zone around the wellbore, becomes negative (in tension) and below the tensile strength (circumferential stress $< T < 0$). Hence, it causes zones of tensile failure on the wellbore wall that are aligned in the S_{Hmax} orientation [*Aadnoy*, 1990;

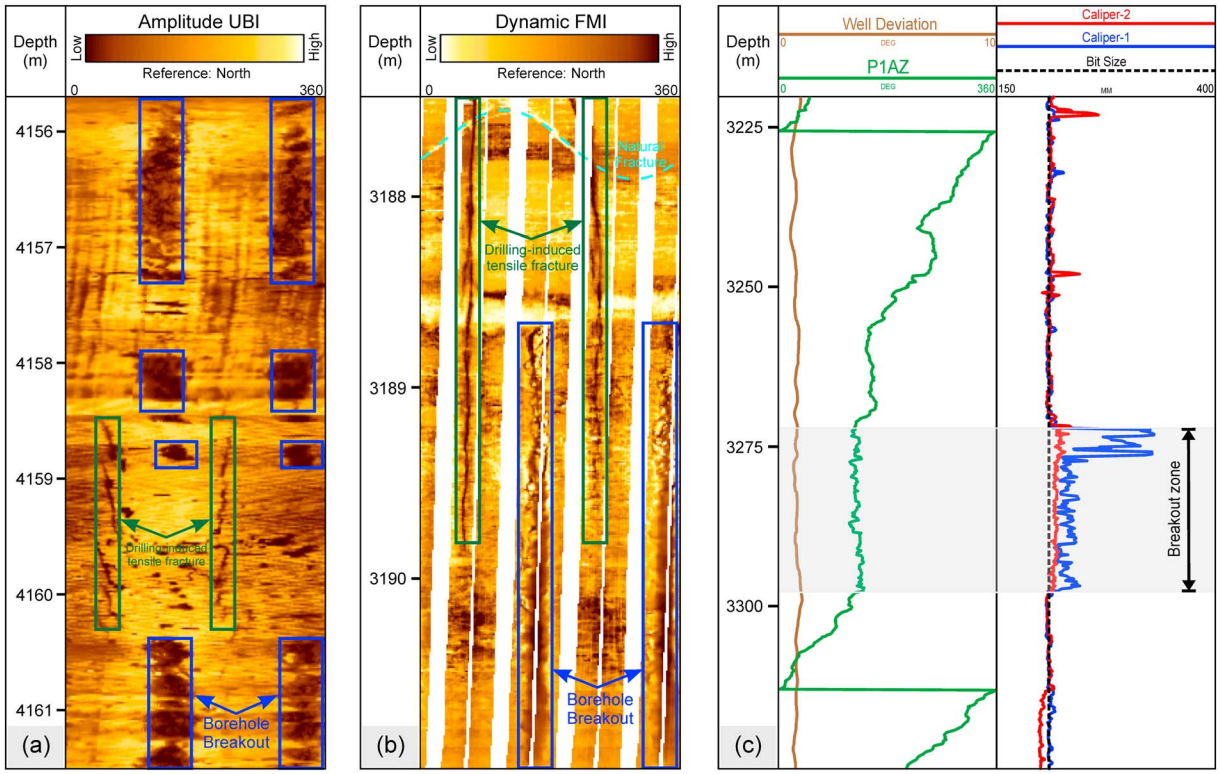

Figure 3. Typical examples of drilling-induced tensile fractures (DIFs) and borehole breakouts (BOs) in acoustic and resistivity borehole image tools. (a) An example of Ultrasonic Borehole Imager (UBI) log from Tekirii-2 well and (b) an example of Fullbore Formation MicroImager (FMI) from Turangi-1 well. In borehole image logs, BOs are defined as poorly resolved wide zones (low-amplitude or conductive zones) due to invasion of drilling mud in the conjugate shear fractures that make an oval shape for the borehole. Note that the BOs and DIFs in vertical wells form in the opposite side of borehole wall. (c) A typical example of BOs in four-arm caliper log in Kupe South well which is characterized by enlargement in one diametrical direction (shown by caliper 1), while the other caliper is similar to bit size. P1AZ is the azimuth of pad 1 relative to magnetic north. Note that interpretation of BOs in caliper logs need particular attention to be distinguished from other types of borehole enlargements (see *Plumb and Hickman* [1985] and *Reinecker et al.* [2003] for more details).

Bell, 1996a; *Zoback*, 2007]. DIFs can be analyzed via borehole image logs as a subset of conductive and subvertical fractures that are observed on opposite sides of the borehole (Figure 3). DIFs cannot be interpreted from oriented caliper logs. In this study, breakout and DIF orientations were corrected for magnetic declination in order to plot the orientations with respect to true north.

3.2. S_{Hmax} Orientation From Earthquake Focal Mechanism Solutions

Natural seismic events (i.e., earthquakes) also provide important information on the state of crustal stress [*Heidbach et al.*, 2010; *McKenzie*, 1969; *Raleigh et al.*, 1972; *Zoback*, 1992]. Three types of seismological indicators are employed in the WSM database to infer the stress state, including single focal mechanisms (FMS), formal stress inversions using several focal mechanisms (FMF), and average or composite focal mechanisms (FMA). The main difference between these indicators is the reliability of the derived stress.

In the FMS method, the orientation of the *P*, *B*, and *T* axes of a focal mechanism solution represents the proximate stress field orientation [*McKenzie*, 1969]. However, the *P*, *B*, and *T* axes are not equal to the principal stress orientations [*Célérier*, 2010; *Heidbach et al.*, 2010; *McKenzie*, 1969]. Assuming that the friction coefficient of the rupture plane is 0.6, the largest principal stress orientation is ~30° off from the rupture plane. Since it is generally not clear which of the two nodal planes is the rupture plane for strike-slip events, the *P* axis bisecting the compressional quadrant of the focal mechanism is used as a proxy for the S_{Hmax} orientation. For the other faulting regimes the other principal axis of the moment tensor are used (see Zoback [1992] for more details). However, theoretically the orientation of the largest principal stress can be anywhere within the compressional quadrant [*Arnold and Townend*, 2007; *McKenzie*, 1969], and thus using the *P* axis as proxy for the stress orientation allows for potentially large uncertainties. Hence, for the WSM database the S_{Hmax} orientation derived from FMS method is assumed to have a standard deviation of ±25° (i.e., C quality

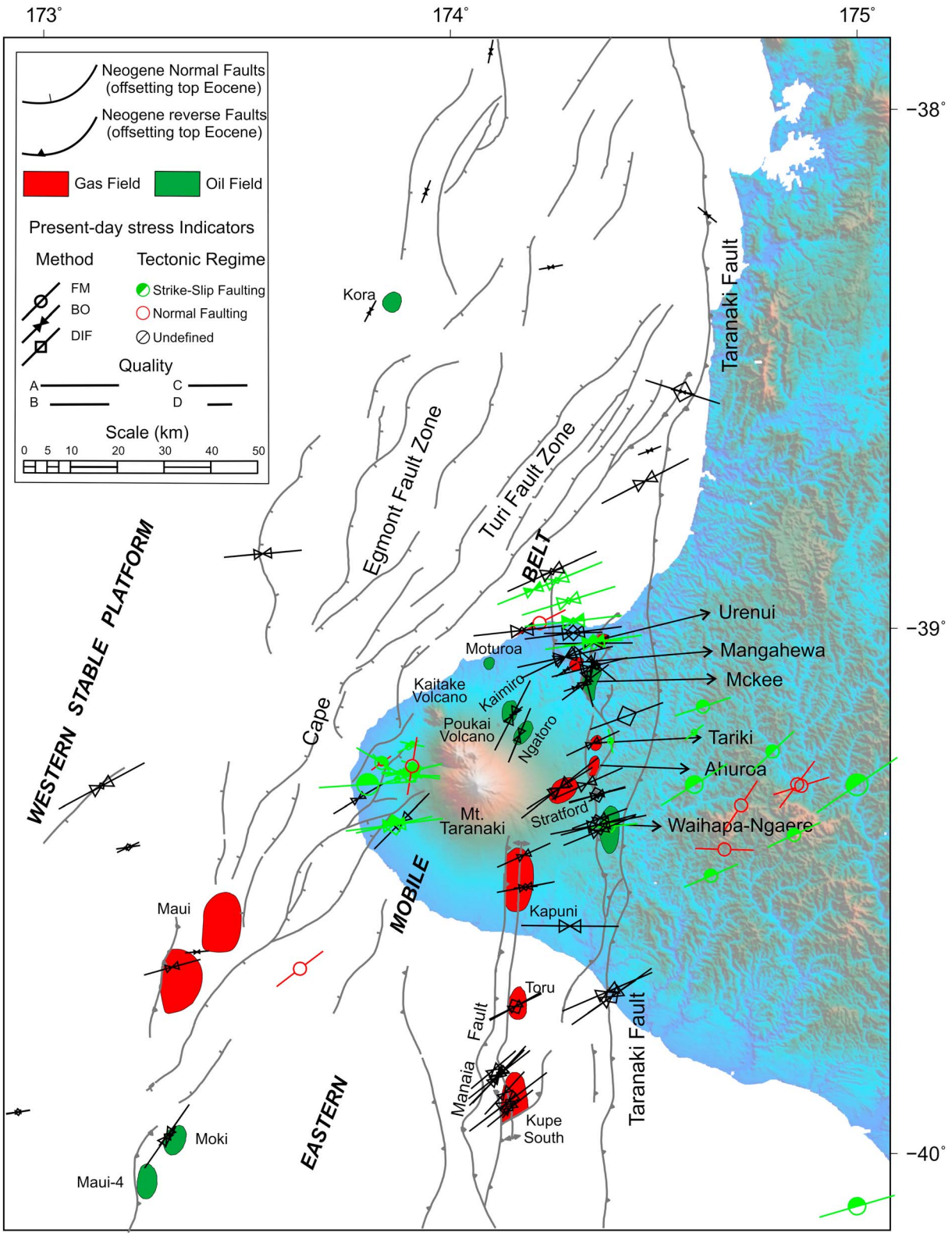

Figure 4. The in situ stress map of the Taranaki Basin. In situ stress data are shown based on the type indicators (FM: focal mechanism solution of earthquakes and stress inversions; DIF: drilling-induced fractures; BO: borehole breakouts) and tectonic stress regime (U: undefined, SS: strike-slip, NF: normal). Lines show the orientation of the S_{Hmax}, and the length of the lines indicates the data quality based on the World Stress Map quality ranking criteria [*Heidbach et al.*, 2010]. Faults and petroleum fields in the Taranaki Basin are from *King and Thrasher* [1996]. Note that the strike-slip stress regime for wellbore data are from *Mildren et al.* [2001] and *GMI* [2010].

Table 1. In Situ Stress Data Indicators in the Taranaki Basin Based on Their Quality and Data Types[a]

	Quality					
Data Type	A	B	C	D	E	Total
Borehole breakouts	18	13	15	19	64	129
Drilling-induced tensile fracture	-	4	5	13	-	22
Focal mechanism solution of earthquakes	-	-	17	16	7	40
Stress inversion of focal mechanisms	2	2	-	-	2	6
Average focal mechanism solutions	-	-	-	1	-	1
Total	20	19	37	49	73	198

[a]The A to E quality is according to the WSM ranking criteria [*Heidbach et al*., 2010].

according to the WSM ranking criteria); [*Heidbach et al*., 2010; *Zoback*, 1992]. The average of *P*, *B*, and *T* axes of several mechanism solutions (i.e., FMA data records [*Leitner et al*., 2001; *Sbar and Sykes*, 1973; *Webb et al*., 1986; *Zoback and Zoback*, 1980]) or the composites [*Sbar et al*., 1972] are less reliable, and thus these data records are assumed to have a higher standard deviation of ±40° and thus receive a D quality in the latest update of the WSM database [*Heidbach et al*., 2010].

A more accurate stress estimation of the principal stress orientations can be achieved with a set of focal mechanism solutions assuming that they are caused by the same stress tensor. Furthermore, this so-called formal stress inversion (FMF) assumes that the earthquake slip direction occurs in the maximum shear stress direction (Wallace-Bott hypothesis [*Bott*, 1959]). Thus, the stress inversion provides the three principal stresses orientation by minimizing the average difference between the slip direction and the maximum shear stress on the inverted faults [*Angelier*, 1984; *Gephart and Forsyth*, 1984; *Michael*, 1984]. This misfit angle is used in the WSM database to assign the data record quality. More recently, *Arnold and Townend* [2007] implemented a probabilistic approach to determine the principal stress axes orientations from earthquake observations. Different inversion methods result in a deviatoric stress tensor, with four parameters including the three principal stress axes orientations and the relative magnitudes of the intermediate principal stress with respect to the minimum and maximum principal stresses. To compare the results of the formal stress inversion with the other data records, the WSM database uses the approach of *Lund and Townend* [2007] to derive the S_{Hmax} orientation from the orientation of the three principal stresses. The stress regime is again assigned using the classification and limits of *Zoback* [1992]. Generally, the S_{Hmax} data records derived from formal inversion of stress receive an A or B quality assignment in the WSM database [*Heidbach et al*., 2010; *Zoback*, 1992].

4. Results: S_{Hmax} Orientation of the Taranaki Basin

In this study we analyzed various types of wellbore image logs, dipmeters, and oriented caliper tools in 129 wells in the Taranaki Basin (Figure 2) to derive the orientation of S_{Hmax} from the interpretation of borehole breakouts and DIFs from 0.8 km to 5 km depths. This analysis results in 151 new A–E quality data records across the basin. In addition, we compiled 40 (A–E quality) FMS data records in the region from published papers by *Webb and Anderson* [1998] and *Sherburn and White* [2006], two FMF data records from *Sherburn and White* [2006], one FMA from *Reyners* [2010], and four FMF data records from *Townend et al*. [2012]. The combination of extensive drilling-induced stress information and focal mechanism solutions of earthquakes allows us to present the first comprehensive contemporary stress map of the Taranaki Basin based on 198 stress indicators. We classified all data records according to the WSM quality ranking criteria, which classifies stress orientations from A to E quality, with A quality being the most reliable and the E quality the least reliable [*Heidbach et al*., 2010]. The details of the Taranaki Basin stress map can be found in Figure 4, Table 1, and the online supporting information.

The earthquake FMS/FMF suggests a deep S_{Hmax} that is generally ranging from E-W to ENE-WSW and indicates both normal and strike-slip stress regimes. The stress orientations from earthquakes are broadly consistent with that observed from breakouts and DIFs, which indicates that S_{Hmax} is usually ~ENE-WSW throughout the basin but does range from NNE-SSW to E-W in individual wells and fields (Figure 4). In the studied wells, we observed localized rotation of breakouts in the vicinity of fractures and faults in the

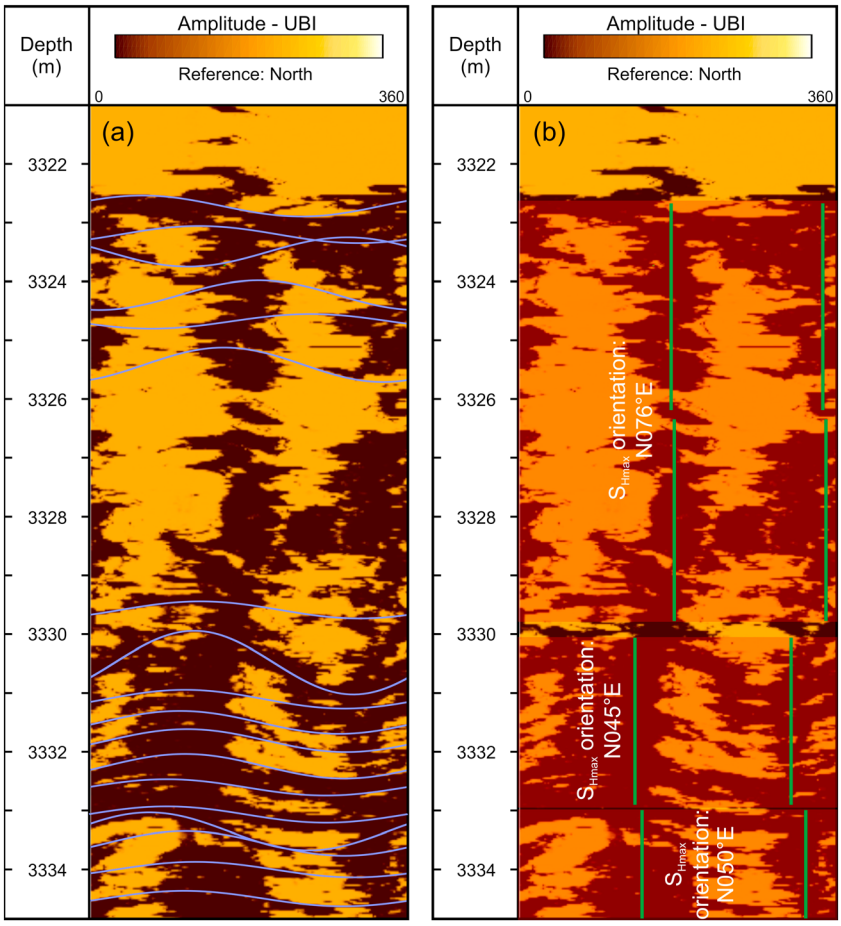

Figure 5. Localized rotation of borehole breakouts (BOs) near faults and fractures in Trapper A-1 well. In this example, (a) blue sinusoids show the interpreted fractures, and (b) green lines indicate the orientation of BOs which is perpendicular to the maximum horizontal stress orientation (S_{Hmax}). The S_{Hmax} orientation is deviated almost 30° in a 10 m depth interval due to presence of faults or high density of natural fractures.

Taranaki Basin (Figure 5). Such a local perturbation of the S_{Hmax} was previously reported in the Taranaki Basin [*Camac et al*., 2005], and other regions worldwide, due to juxtaposition of different types of rocks, slip on active faults, and changes in the rock mechanical properties owing to high density of fractures [*Rajabi et al*., 2016a, 2016b; *Zoback*, 2007]. It should be noted that local perturbations of breakouts in the studied wells occur in very short intervals (e.g., 10–15 m; Figure 5) and do not have a significant impact on the mean S_{Hmax} orientation.

In order to analyze the pattern of the mean basin-wide S_{Hmax} orientation, we applied two different methods, including stress province determination from Rayleigh test [*Hillis and Reynolds*, 2000; *Rajabi et al*., 2016b] and the stress smoothing technique [*Coblentz and Richardson*, 1995; *Hansen and Mount*, 1990; *Heidbach et al*., 2010; *Müller et al*., 2003; *Reiter et al*., 2014]. In the stress province method demonstrated by *Hillis and Reynolds* [2000], the data records in the basin are weighted based on their quality. The most reliable S_{Hmax} data record, A quality data, received a weight of 4 down to D quality that received a weight of 1. Often, only the A–C quality data are considered as reliable data records, while D quality data records are less reliable because D quality data have a higher probability to reflect local perturbations of the S_{Hmax} orientation rather than long-wavelength S_{Hmax} orientation [*Heidbach et al*., 2010]. However, there are several examples that demonstrate the potential reliability of D quality data records in different regions worldwide. For example, *Tingay et al*. [2010], *Reiter et al*. [2014], and *Ziegler et al*. [2016] clearly demonstrated that the inclusion of D quality data records does not increase the overall stress variability compared to only A–C data interpretation and that the inclusion of D quality data can yield a more representative regional stress orientation in

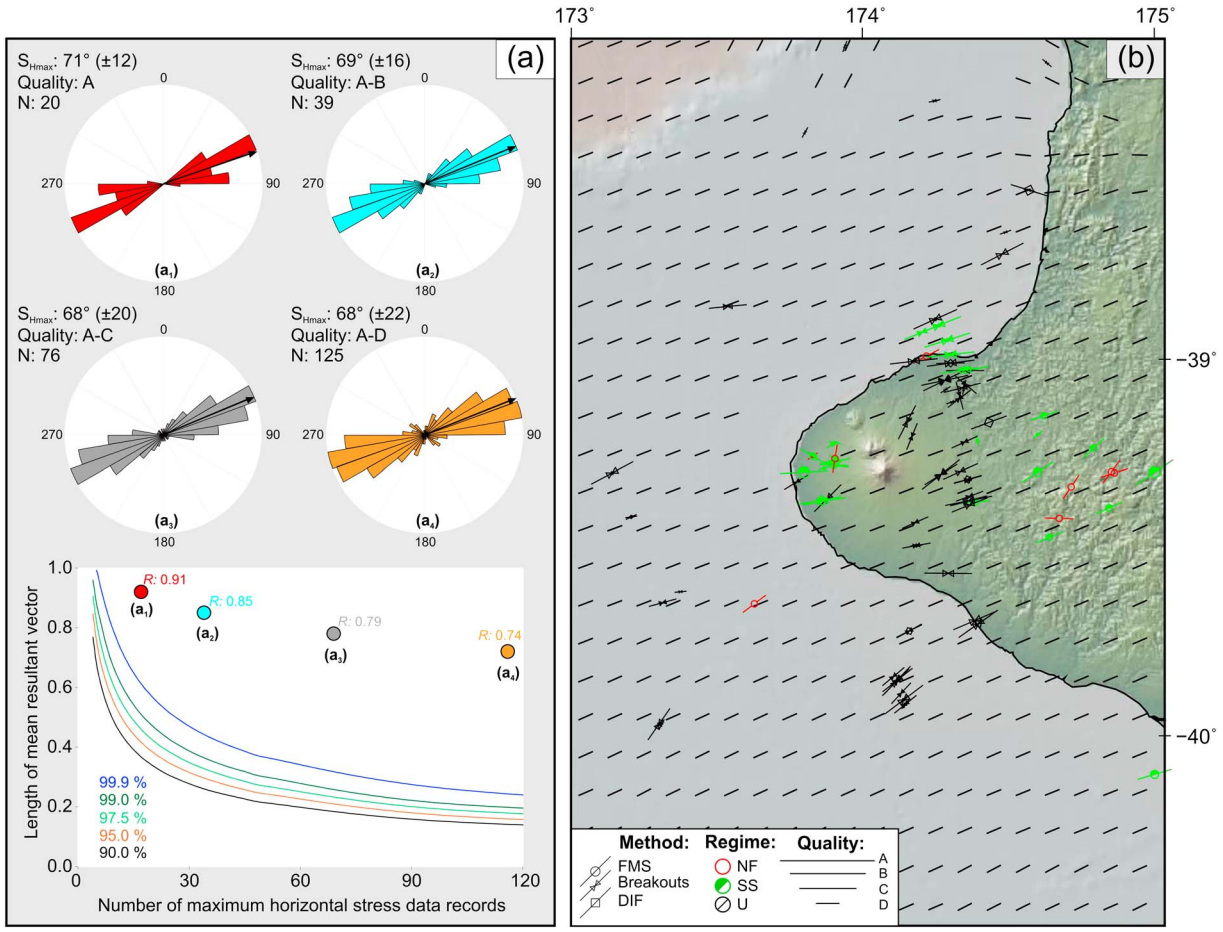

Figure 6. Statistical analysis of the mean orientation of S_{Hmax} across the Taranaki Basin. (a) Different rose diagrams show the distribution of S_{Hmax} orientations for different data sets [*Heidbach et al*., 2010] which show consistent S_{Hmax} orientation with and without D quality data. Plot in Figure 6a shows the Rayleigh test for the data records in the Taranaki Basin. Different lines in this plot are based on the cutoff values of *Mardia* [1972]. In order to do this statistical test, we first calculated length of resultant vector for each data set and plotted it versus number of data records. As can be seen, in all situations (using different WSM qualities) the mean S_{Hmax} orientation across the Taranaki Basin is statistically significant because they pass the highest line (i.e., 99.9%). (b) Smoothing the mean S_{Hmax} orientation on a 0.1° grid as described by *Heidbach et al*. [2010]. See text for the details of this method. Note the local deviation due to the topography of the Egmont Volcano (Mount Taranaki) where the smoothed mean S_{Hmax} orientation has more than 25° SD and, hence, is not plotted.

sedimentary basins. However, it should also be noted that some other studies have suggested that it can be unreliable to include D quality data for the understanding of regional stress pattern, as these data can result in an increase in stress variability due to presence of local structures that show the local pattern of stress [*Rajabi et al*., 2016a; *Rajabi et al*., 2016b]. Extreme caution needs to be exercised to refrain from filtering of data records, simply because they do or do not "fit" preconceived expectations. As a rule of thumb, high-quality borehole image logs, which may only include a few meters of stress indicators, often provide locally highly reliable stress information even though the individual stress data record is assigned a D quality, using the WSM criteria, because of the small number or short length of observed stress indicators.

In order to assess the reliability of D quality data in the Taranaki Basin, we calculated the mean S_{Hmax} orientation, length of the mean resultant vector (R bar), and the standard deviation (SD) with and without D quality data. We then applied the Rayleigh test [*Coblentz and Richardson*, 1995; *Davis*, 2002; *Mardia*, 1972] on different sets of stress data records to check if the mean S_{Hmax} orientations across the Taranaki Basin are distributed randomly or systematically. The result of the stress province calculations are presented in Figure 6 and show a prevailing ENE-WSW S_{Hmax} orientation across the Taranaki Basin with generally low SD values regardless of the inclusion of D quality data in the statistical calculations. Thus, we conclude that the D quality data reliably show the S_{Hmax} orientation across the basin and hence we included them for smoothing analysis in the following section.

Table 2. Comparison Between the Calculated Maximum Horizontal Stress Orientations (S_{Hmax}) Inferred From Single Focal Mechanism Solutions of Earthquakes (FMS), Stress Inversions of Focal Mechanisms (FMF), and Wellbore Data[a]

	No. of Data Records				Mean S_{Hmax} (A–C Quality Data Records)		Mean S_{Hmax} (A–D Quality Data Records)	
Data Records	A	B	C	D	Weighted	Unweighted	Weighted	Unweighted
Wellbore indicators	18	17	20	32	068° (±19°)	067° (±20°)	067° (±21°)	066° (±24°)
FMF	2	2	0	0	069° (±13°)	069° (±13°)	069° (±13°)	069° (±13°)
FMS and FMA	0	0	17	17	067° (±27°)	067° (±27°)	072° (±30°)	076° (±33°)

[a]To calculate the weighted mean S_{Hmax} orientation, A quality receives a weight of 4 down to D quality which receives weight of 1. The mean S_{Hmax} orientations (calculated by bipolar statistics) show similar results between wellbore and FMS/FMF data. However, D quality FMS data increases standard deviation, and, hence, lower weight should be put on these data records. Note that A–D qualities are the World Stress Map quality ranking [*Heidbach et al*., 2010].

The smoothing analysis of stress pattern calculates the mean S_{Hmax} orientation, and its variability, on a grid map for different search radii [*Heidbach et al*., 2010; *Müller et al*., 2003; *Reiter et al*., 2014]. In this study, we used the algorithms developed by *Heidbach et al*. [2010] to calculate the smoothed S_{Hmax} pattern across the Taranaki Basin on a 0.1° grid. Each data record was weighted according to its quality and the inverse distance from each grid point. We plotted the mean S_{Hmax} orientation at the grid point when at least three S_{Hmax} orientations were within the search radius and when the SD is $< 25°$. Figure 6 illustrates the smoothed stress pattern across the study area from this analysis, which confirms the general ENE-WSW S_{Hmax} trend for the Taranaki Basin region. It should be noted that each plotted mean S_{Hmax} orientation is reliable within ± 25°.

5. Discussions

5.1. The Pattern of In Situ Stress in the Taranaki Basin

Previous studies of the stress pattern of the Taranaki Region were based mainly on the earthquake FMS data [*Cavill et al*., 1997; *Reyners*, 1980; *Sherburn and White*, 2006; *Townend et al*., 2012; *Webb and Anderson*, 1998] and with particular emphasis on the seismicity of the Egmont Volcano (Mount Taranaki). *Sherburn and White* [2006] suggested an east-west S_{Hmax} orientation in the Taranaki region based on 39 FMS data and two FMF analyses, despite this direction not being consistent with the NW-SE extension inferred from recent geological data. Thus, they suggested that the volcanic activity of Mount Taranaki was possibly perturbing the stress field in the area [*Sherburn and White*, 2006]. Furthermore, they noted a high angle between their regional E-W S_{Hmax} and the strike of the CEFZ (~N45°E), and concluded that this fault system must contain high pore fluid pressure or have a low coefficient of friction [*Sherburn and White*, 2006]. According to our analysis, based on 129 wellbore and 47 FMS/FMF/FMA data, the regional pattern of stress across the basin is N68°E (±22°) which is slightly different from what was suggested by *Sherburn and White* [2006] and is more broadly consistent with both the regional extension direction and the strike of the CEFZ.

In this study, we assessed the FMS data of *Sherburn and White* [2006] using the WSM quality ranking criteria [*Heidbach et al*., 2010]. This led to seven data records receiving E quality because no clear tectonic regime could be established according to *Zoback* [1992]. This means that the *P*, *B*, and *T* axes are rather oblique, which prevents a conclusive derivation of a tectonic stress regime, and hence no assignment of a S_{Hmax} is possible. Therefore, these data records are not included in our database. We then compared the mean S_{Hmax} orientation of the region inferred from FMS, FMF, and wellbore data separately to see if these three different methods provide similar results. To calculate the mean S_{Hmax} orientation for these three different data sets, we first calculated the mean S_{Hmax} for all the data regardless of their quality (unweighted in Table 2). We then put more weight on more reliable data records (A = 4, B = 3, C = 2 and D = 1) and calculated the mean S_{Hmax} orientation (weighted in Table 2). The results reveal similar values for the mean S_{Hmax} orientation derived from A–C quality wellbore and FMF and FMS data (Table 2). However, D quality FMS data records result in more standard deviations on the mean S_{Hmax} orientation. Hence, putting lower weight on the poor quality data (such as D quality FMS) is recommended for the calculation of mean S_{Hmax} orientations. The comparison between wellbore and earthquake data has been investigated before in other regions, such as Italy as convergent plate boundaries [*Pierdominici and Heidbach*, 2012], Iceland as divergent plate boundaries [*Ziegler et al*., 2016], and southwest of Iran as a continental collision zone

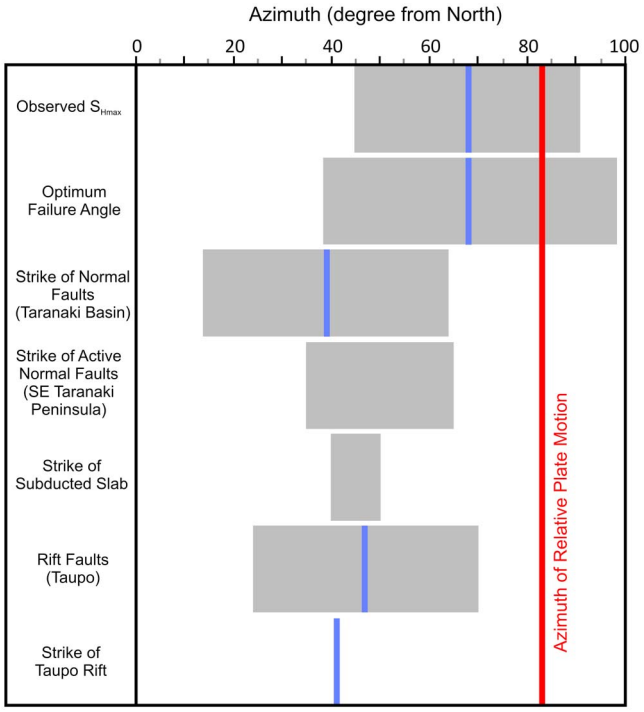

Figure 7. Summary and comparison between observed maximum horizontal stress orientation (S_{Hmax}) and other azimuthal data in and around the Taranaki Basin. Each line shows the mean azimuth, and the shaded areas are standard deviation. The optimum failure angle is determined as the mean S_{Hmax} orientation ±30°. Strike of normal faults in Taranaki Basin and south of Taranaki Peninsula are from *Giba et al.* [2010] and *Townsend et al.* [2010], respectively. The geometry of slab and strike of Taupo rift are from *Seebeck et al.* [2013, 2014]. All these azimuthal features are interrelated because they are caused by or are consequences of the in situ stress field and the plot shows that most of the data are consistent with each other.

[*Rajabi et al.*, 2010, 2014]. Therefore, our results, that is, from the near subduction zone, confirm that these two very different methods result in the same mean S_{Hmax} orientation within the standard deviation.

5.2. Comparisons Between the Stress Pattern and Geological Data in the Taranaki Basin

There have been extensive studies on the geometry and kinematics of faults in the North Island and the Taranaki Basin [*Giba et al.*, 2010, 2013; *Reilly et al.*, 2015; *Seebeck et al.*, 2013, 2014]. For example, *Giba et al.* [2010], in a detailed study on the evolution of the northern Taranaki Basin, suggested a regional NE-SW strike for Late Miocene and younger faults. Furthermore, they documented a southward migration of normal faults in the northern Taranaki Basin, where older faults (formed between 12 and 4 Ma) in the north show a regional trend of ~N19°E, while younger faults (<4 Ma) in the south show a regional trend of ~N41°E [*Giba et al.*, 2010]. In addition, kinematic analyses of normal fault outcrops along the northern Taranaki coast suggest NW-SE extension for the faults that were active between 0.3 and 5 Ma, which is consistent with regional fault strikes [*Giba et al.*, 2010].

Townsend et al. [2010] characterized the recurrence rate, timing, and magnitude of six active normal faults to the southwest of Mount Taranaki. These active faults show a regional NE-SW to ENE-WSW trend (varies between N35°E and N65°E) and indicate paleoseismicity with magnitudes of > 6 for these faults. The tectonic or volcanic origin of these faults was discussed by *Townsend et al.* [2010], and they suggested that the faults were formed due to tectonic activity because they were probably active before the volcanic activity. The consistency between our determined S_{Hmax} orientation and the trend of these faults further supports a tectonic origin for these faults (Figure 7). *Reilly et al.* [2015] showed NNE-SSW and ENE-WSW trending normal faults west and east of the CEFZ, respectively. The presence of NE-SW reverse faults was also reported in the southwest of North Island and north of South Island which is consistent with NW-SE to WNW-ESE S_{Hmax} orientation for that region determined by *Townend et al.* [2012]. *Seebeck et al.* [2014] also suggested a NE-SW trend for active normal faults of the Taupo Rift Zone (east of the Taranaki Basin), where kinematic data show a mean extension of S43°E (±23). Generally, most of the studies in the Taranaki Basin, and active intra-arc rift in the central North Island, suggest significant NW-SE extension on the NE trending faults, which is consistent with the regional N68°E (±22°) S_{Hmax} orientation determined in his study (Figure 7).

According to the earthquake FMS data, a strike-slip tectonic stress regime primarily exists in the region but with some suggestions of a normal faulting stress regime, particularly in the eastern part of the basin, and these stress regimes are consistent with the rifting nature of the central North Island. For example, *McNamara et al.* [2015] suggested a NE-SW S_{Hmax} orientation and normal stress regime in the eastern side of the Taranaki region in three geothermal wells in the Rotokawa Geothermal Field, which the predicted

S_{Hmax} is subparallel to the active rift axis. Several unpublished petroleum reports determined stress regime in different parts of the Taranaki Basin. For example, *Mildren et al*. [2001] predicted a broadly strike-slip stress regime in the normally and mildly overpressure zones of the Pohokura Field (offshore of the northern Taranaki Basin). However, their predicted S_{Hmax} magnitude in the overpressure zone is similar to S_v ($S_{Hmax}/S_v = 1.03$), and thus this stress regime may be better classified as a borderline strike-slip/normal faulting stress regime. *Mildren and Meyer* [2006] determined a strike-slip stress regime in Moana Prospect (northern Taranaki Graben). *Mildren* [2009] investigated the stress regime in the Mangatoa area (northern Taranaki) and found that the magnitude of S_v and S_{Hmax} are similar above the overpressure zone, and stress conditions verge on the transition between normal and strike-slip stress regimes. Similarly, *GeoMechanics International Inc. (GMI)* [2010] also predicted a strike-slip faulting regime for the Te Kiri Prospect in the Western Taranaki Peninsula (Figure 4). Hence, petroleum data also suggest a generally strike-slip regime and, in some cases, a transition from strike-slip to normal stress regime. The accommodation of strike-slip component on the normal faults in the Taupo Rift Zone (east of Taranaki Basin) has also been suggested and is consistent with petroleum data [*Acocella et al*., 2003; *Lamarche et al*., 2005; *Nairn and Cole*, 1981; *Seebeck et al*., 2013; *Spinks et al*., 2005].

5.3. Controls on the Stress Pattern of the Taranaki Basin

Deformation and tectonic setting of the North Island is mainly controlled by the Pacific Plate subduction beneath the Indo-Australian Plate [*Nicol and Beavan*, 2003; *Nicol et al*., 2007; *Nicol and Wallace*, 2007; *Townend et al*., 2012; *Wallace et al*., 2004]. The process of the subduction in the North Island can be traced by several features such as folds and faults in the eastern portion (fore arc), active intra-arc rift (and associated volcanism in the Taupo rift zones) and back-arc spreading in the central and central western part of North Island [*Nicol and Beavan*, 2003; *Nicol et al*., 2007; *Nicol and Wallace*, 2007; *Townend et al*., 2012; *Wallace et al*., 2004]. The convergence of the plates at the Hikurangi margin is oblique and, due to slab rollback, induces trench-parallel and trench-perpendicular suction forces that control the stress state of the overriding plate [*Barnes et al*., 1998; *Townend et al*., 2012; *Wallace et al*., 2004].

As outlined in the previous section, comprehensive studies on the evolution of volcanism, rifting, and faulting in the Taranaki Basin suggest NE-SW trending active and recent normal faults that are broadly consistent with our observed S_{Hmax} orientation. Although most of the faults in the northern part of the Taranaki Basin show a NE-SW trend, *Giba et al*. [2010] clearly demonstrated that normal faults with NNE-SSW orientation were active between 12 and 4 Ma, while younger faults (0–4 Ma) that are primarily present in the southern part of the basin show clockwise changes in their strikes. In the northern Taranaki Basin, *Giba et al*. [2010] determined a regional trend of N39°E (±25°) for the normal faults, which is generally consistent with our determined N68°E (±22°) S_{Hmax} orientation (Figure 7). Furthermore, this ENE-WSW S_{Hmax} orientation is fully consistent with the trend of normal faults at the southern Taranaki Basin [*Reilly et al*., 2015] and outcrop normal faults in the southeast of the Taranaki Peninsula [*Townsend et al*., 2010] (Figure 7). Note that most of the active faults in the Taranaki Basin were originally initiated during past tectonic phases and have been reactivated due to episodic extensions and contractions [*Giba et al*., 2010; *Giba et al*., 2013; *King and Thrasher*, 1996; *Reilly et al*., 2015; *Sherburn and White*, 2006]. Hence, their orientation of active faults may not be optimally oriented with the exact present-day S_{Hmax} orientation [*Sherburn and White*, 2006].

The regional ENE-WSW orientation of S_{Hmax} in the Taranaki Basin is subparallel to the relative motion of Pacific and Australian plates (Figure 7). If we consider the transmission of this relative motion as the main source of the contemporary tectonic stress in the Taranaki Basin, we would predict that a prevailing thrust stress regime exists in the region. However, as outlined above, most of the Taranaki Basin (except in the northernmost of part of South Island) shows a strike-slip to normal stress regime. At a tectonic plate scale, the strike of the subducted slab beneath the central western North Island is N40°E–N50°E (Figure 7) [*Seebeck et al*., 2013; *Seebeck et al*., 2014]. The trend of the slab in the vicinity of the Taranaki Basin (~N50°E) is almost subparallel with the pattern of S_{Hmax} orientation (N68°E). Similar effects of slab orientation on stress patterns are observed in other subduction zones such as Hellenic Arc in the Mediterranean [*Doutsos and Kokkalas*, 2001; *Heidbach et al*., 2010; *Meijer and Wortel*, 1997] and Cascadia subduction zone [*Balfour et al*., 2011; *Wang*, 2000] where there is a margin-normal S_{Hmax} orientation at the subduction front and a margin-parallel S_{Hmax} orientation farther from the trench and in the back-arc region.

The standard deviation of our determined S_{Hmax} orientation is ±22° and can explain the ~20° difference between regional strike of the slab and the S_{Hmax} orientation (Figure 7). However, two other stress sources can also be suggested to explain this ~20° difference. First, the clockwise rotation of the North Island around a vertical axis could be an alternative cause of this ~20° difference (Figure 7). Several studies have proposed clockwise rotation of the North Island around a vertical axis due to a variable rollback process of the subducting plate and the southward transition of subduction to continental collision along the Hikurangi margin. In this region, the Pacific Plate is being subducted in the northern part of the margin (slab rollback dominant), while there is a continental collision zone in the southern part due to the presence of a buoyant indenter and the unsubductable Chatham Rise [*Beavan and Haines*, 2001; *Nicol et al*., 2007; *Nicol and Wallace*, 2007; *Walcott*, 1987; *Wallace et al*., 2004, 2009]. Second, *Stern et al*. [2013] suggested mantle dripping in the western North Island where there are sharp lithospheric changes across the Taranaki-Ruapehu line. These sharp changes are also present in the recent Moho map of New Zealand [*Salmon et al*., 2013] where the Moho depth in southwest of North Island is thicker than the Moho in the Taranaki region. These lithospheric changes along with mantle dripping probably provide gravitational instabilities and can affect the stress pattern of the Taranaki Basin.

Seebeck et al. [2013] comprehensively investigated the geometry and strike of the subducted Pacific Plate beneath the Australian Plate in the last 20 Ma and suggested a consistent trend for the slab since 16 Ma, which is not in agreement with clockwise rotation of the overriding plate. Consequently, *Seebeck et al*. [2013] proposed that the clockwise rotation of the North Island is independent of the subducted slab and occurs due to decoupling deformation between the plates owing to the accommodation of the majority of relative plate motion by subduction thrust at Hikurangi margin. Hence, similar to *Seebeck et al*. [2014], who concluded that the geometry of the subducted slab provides the major control on the geometry of rift faults in the Taupo Rift Zone, we suggest that the state of in situ stress in the Taranaki Basin is mainly controlled by rollback of the subducting slab and the associated force of subduction suction.

5.4. Implications for Petroleum Exploration

The Taranaki Basin has significant economic importance because it is the major petroleum province of New Zealand. The implications of the present-day stress, particularly the S_{Hmax} orientation, have been demonstrated in numerous studies from early exploration to field abandonment [*Bell*, 1996b; *Tingay et al*., 2005; *Zoback*, 2007]. The information of the present-day stress has major applications in wellbore stability, fault seal and fracture permeability, sand production prediction, and subsurface fluid flow [*Barton et al*., 1995; *Bell*, 1996b; *Heffer et al*., 1997; *Tingay et al*., 2005; *Zoback*, 2007]. The understanding of the present-day stress in the Taranaki Basin is particularly important because it is a rifted basin, where faults and fractures play critical roles in different aspects of the petroleum exploration and production. Generally, the concept of structural permeability [*Sibson*, 1996] demonstrates the fluid-flow ability of fractures and faults that are oriented subparallel to the orientation of the S_{Hmax} [*Barton et al*., 1995; *Zoback*, 2007]. The failure angle is defined as the angle between the S_{Hmax} orientation and strike of faults, which *Sibson* [1985] suggested as being 22.5–30° for typical friction coefficients of 0.6–1.0 [*Byerlee*, 1978]. In a normal stress regime, the optimal orientated faults are parallel to S_{Hmax} orientation. *Sherburn and White* [2006] considered the strike of CEFZ as N45°E and determined an east-west orientation for the S_{Hmax} across the Taranaki Basin. Hence, they found a large failure angle for the Taranaki region (i.e., $>$30°) and concluded high pore fluid pressure or a low coefficient of friction of the faults in the region.

Our refined stress map of the Taranaki Basin suggests that interpreted faults are in the optimum range of failure angle (Figure 7). In addition, neotectonic information generally suggests a normal faulting stress regime in the Taranaki Basin [*Giba et al*., 2010; *Litchfield et al*., 2013; *Townsend et al*., 2010], while unpublished wellbore data [*GMI*, 2010; *Mildren*, 2009; *Mildren and Meyer*, 2006] and earthquake FMS data [*Sherburn and White*, 2006] suggest both strike-slip and normal stress regimes in the basin. We did not observe any systematic changes of stress regime in the Taranaki Basin laterally and with depth. Hence, the presence of two tectonic stress regimes across the basin possibly is due to the existence of geological structures, density contrasts, mantle dripping, and the Mount Taranaki activity. The existence of normal and strike-slip stress regime have significant implications for wellbore stability of the Taranaki Basin, where erroneous assessment of present-day stresses can lead to expensive instability or collapse of boreholes [*Tingay et al*., 2015; *Zoback*, 2007].

The orientation of the S_{Hmax} can be deviated from the regional trend, laterally and with depth, due to the presence of geological features [*Rajabi et al*., 2016a, 2016b; *Zoback*, 2007]. The Taranaki Basin shows a significant ENE-WSW S_{Hmax} orientation except the west of Mount Taranaki where a number of close by indicators show rotations from the regional trend possibly owing to density contrast and magmatism as previously highlighted by *Sherburn and White* [2006]. Localized perturbation of stress, with depth, has been previously reported in the vicinity of intersected faults in the Taranaki Basin [*Camac et al*., 2005]. We also observed these small-scale stress rotations at short intervals in some of the studied wells (Figure 5). These localized stress variations can have significant implications in geomechanical characterization of georeservoirs [*Bell*, 1996b; *Rajabi et al*., 2016b; *Zoback*, 2007]. The orientation of S_{Hmax} is an important issue in the initiation of induced hydraulic fractures and an effective method for stimulation of hydrocarbon and geothermal reservoirs [*Bell*, 1996b; *Zoback*, 2007]. Hence, localized deviation of stress due to small-scale stress sources can initiate complex and ineffective hydraulic fracture stimulations [*Maxwell et al*., 2009; *Rajabi et al*., 2016b]. This issue is particularly important for the Taranaki Basin where hydraulic fracturing stimulation is implemented to extract oil from reservoir rocks in some fields [*Green et al*., 2006].

6. Conclusions

This paper presents the first comprehensive contemporary stress map of the Taranaki Basin of New Zealand, which is located on the Australian Plate adjacent to the Pacific-Australian plate boundary. The interpretation of wellbore and earthquake data provides a mean S_{Hmax} orientation of N68°E (±22°) across the Taranaki Basin, which is consistent with NW-SE extension of the region suggested by subsurface and outcrop published geological data. The mean S_{Hmax} orientation is almost parallel to the strike of the subduction trench and the subducting slab, indicating that the subduction process of the Pacific Plate is the most likely key control on the pattern of stress in the Taranaki Basin. In addition to the dominant regional stress orientation driven by the adjacent subduction zone, we also observed small-scale stress perturbations (localized rotation of breakouts) in the vicinity of small-scale geological sources, as well as close to the density contrast of the Egmont Volcano (Mount Taranaki). The regional and local stress orientation, which has numerous implications in geomechanical studies, is important to explain the impact of smaller-scale sources of stress even in the presence of large-scale plate boundary forces.

Acknowledgments

The authors gratefully thank the New Zealand Petroleum & Minerals, Ministry of Business, Innovation & Employment (http://www.nzpam.govt.nz) for providing the raw data of this study. This research forms part of ARC Discovery Project DP120103849 and ASEG Research Foundation Project RF13P02. The authors also would like to thank the Ikon Science in Adelaide (formerly JRS Petroleum Research) for the use of their JRS suite. M. Giba is thanked for providing the fault data in the Taranaki Basin. We also specially thank Martha Savage, John Townend, and an anonymous reviewer of this article for their constructive comments.

References

Aadnoy, B. S. (1990), In-situ stress directions from borehole fracture traces, *J. Pet. Sci. Eng.*, *4*(2), 143–153, doi:10.1016/0920-4105(90)90022-U.

Acocella, V., K. Spinks, J. Cole, and A. Nicol (2003), Oblique back arc rifting of Taupo Volcanic Zone, New Zealand, *Tectonics*, *22*(4), 1045, doi:10.1029/2002TC001447.

Anderson, E. M. (1905), The dynamics of faulting, *Trans. Edinb. Geol. Soc.*, *8*, 387–402.

Anderson, H., and T. Webb (1994), New Zealand seismicity: Patterns revealed by the upgraded National Seismograph Network, *New Zeal. J. Geol. Geop.*, *37*(4), 477–493, doi:10.1080/00288306.1994.9514633.

Angelier, J. (1984), Tectonic analysis of fault slip data sets, *J. Geophys. Res.*, *89*(B7), 5835–5848, doi:10.1029/JB089iB07p05835.

Arnold, R., and J. Townend (2007), A Bayesian approach to estimating tectonic stress from seismological data, *Geophys. J. Int.*, *170*(3), 1336–1356, doi:10.1111/j.1365-246X.2007.03485.x.

Balfour, N. J., J. F. Cassidy, S. E. Dosso, and S. Mazzotti (2011), Mapping crustal stress and strain in southwest British Columbia, *J. Geophys. Res.*, *116*, B03314, doi:10.1029/2010JB008003.

Barnes, P. M., B. M. de Lépinay, J.-Y. Collot, J. Delteil, and J.-C. Audru (1998), Strain partitioning in the transition area between oblique subduction and continental collision, Hikurangi margin, New Zealand, *Tectonics*, *17*(4), 534–557, doi:10.1029/98TC00974.

Barton, C. A., M. D. Zoback, and D. Moos (1995), Fluid flow along potentially active faults in crystalline rock, *Geology*, *23*(8), 683–686, doi:10.1130/0091-7613(1995)023<0683:ffapaf>2.3.co;2.

Beavan, J., and J. Haines (2001), Contemporary horizontal velocity and strain rate fields of the Pacific-Australian plate boundary zone through New Zealand, *J. Geophys. Res.*, *106*(B1), 741–770, doi:10.1029/2000JB900302.

Beavan, J., P. Tregoning, M. Bevis, T. Kato, and C. Meertens (2002), Motion and rigidity of the Pacific Plate and implications for plate boundary deformation, *J. Geophys. Res.*, *107*(B10), 2261, doi:10.1029/2001JB000282.

Bell, J. S. (1990), Investigating stress regimes in sedimentary basins using information from oil industry wireline logs and drilling records, *Geol. Soc. London Spec. Pub.*, *48*(1), 305–325, doi:10.1144/gsl.sp.1990.048.01.26.

Bell, J. S. (1996a), Petro Geoscience 1. In situ stresses in sedimentary rocks (part 1): Measurement techniques, *Geosci. Can.*, *23*(2), 85–100.

Bell, J. S. (1996b), Petro Geoscience 2. In situ stresses in sedimentary rocks (part 2): Applications of stress measurements, *Geosci. Can.*, *23*(3), 135–153.

Bell, J. S., and D. I. Gough (1979), Northeast-southwest compressive stress in Alberta evidence from oil wells, *Earth Planet. Sci. Lett.*, *45*(2), 475–482, doi:10.1016/0012-821X(79)90146-8.

Bird, P. (2003), An updated digital model of plate boundaries, *Geochem. Geophys. Geosyst.*, *4*(3), 1027, doi:10.1029/2001GC000252.

Bott, M. H. P. (1959), The mechanics of oblique slip faulting, *Geol. Mag.*, *96*(2), 109–117.

Byerlee, J. (1978), Friction of rocks, *Pure Appl. Geophys.*, *116*(4-5), 615–626, doi:10.1007/BF00876528.

Camac, B., S. P. Hunt, C. E. Gilbert, and D. P. Anthony (2005), Using 3D distinct element method to predict stress distribution – Kupe Field, Taranaki Basin, New Zealand, in *67th EAGE Conference & Exhibition*, 5 pp., Madrid, Spain.

Cavill, A. W., J. Cassidy, and B. J. Brennan (1997), Results from the new seismic monitoring network at Egmont Volcano, New Zealand: Tectonic and hazard implications, *New Zeal. J. Geol. Geop.*, *40*(1), 69–76, doi:10.1080/00288306.1997.9514741.
Célérier, B. (2010), Remarks on the relationship between the tectonic regime, the rake of the slip vectors, the dip of the nodal planes, and the plunges of the *P*, *B*, and *T* axes of earthquake focal mechanisms, *Tectonophysics*, *482*(1–4), 42–49, doi:10.1016/j.tecto.2009.03.006.
Coblentz, D. D., and R. M. Richardson (1995), Statistical trends in the intraplate stress field, *J. Geophys. Res.*, *100*(B10), 20,245–20,255, doi:10.1029/95JB02160.
Coblentz, D. D., S. Zhou, R. R. Hillis, R. M. Richardson, and M. Sandiford (1998), Topography, boundary forces, and the Indo-Australian intraplate stress field, *J. Geophys. Res.*, *103*(B1), 919–931, doi:10.1029/97JB02381.
Davis, J. C. (2002), *Statistics and Data Analysis in Geology*, 3rd ed., pp. 656, Wiley, New York.
DeMets, C., R. G. Gordon, and D. F. Argus (2010), Geologically current plate motions, *Geophys. J. Int.*, *181*(1), 1–80, doi:10.1111/j.1365-246X.2009.04491.x.
Doutsos, T., and S. Kokkalas (2001), Stress and deformation patterns in the Aegean region, *J. Struct. Geol.*, *23*(2–3), 455–472, doi:10.1016/S0191-8141(00)00119-X.
Engelder, T. (1993), *Stress Regimes in the Lithosphere*, Princeton Univ. Press, New Jersey.
Gephart, J. W., and D. W. Forsyth (1984), An improved method for determining the regional stress tensor using earthquake focal mechanism data: Application to the San Fernando Earthquake Sequence, *J. Geophys. Res.*, *89*(B11), 9305–9320, doi:10.1029/JB089iB11p09305.
Giba, M., A. Nicol, and J. J. Walsh (2010), Evolution of faulting and volcanism in a back-arc basin and its implications for subduction processes, *Tectonics*, *29*, TC4020, doi:10.1029/2009TC002634.
Giba, M., J. J. Walsh, A. Nicol, V. Mouslopoulou, and H. Seebeck (2013), Investigation of the spatio-temporal relationship between normal faulting and arc volcanism on million-year time scales, *J. Geol. Soc.*, *170*(6), 951–962, doi:10.1144/jgs2012-121.
GeoMechanics International Inc. (GMI) (2010), Te Kiri prospect geomechanical analysis, PEP 51149, *Ministry of Economic Development New Zealand Unpublished Petroleum Report PR4278*, 127.
Green, D., K. Seanard, and A. N. Martin (2006), Hydraulic fracturing of Miocene and Oligocene sandstones in the Taranaki Basin, New Zealand, in *SPE Asia Pacific Oil & Gas Conference and Exhibition*, edited, Society of Petroleum Engineers, Adelaide, Australia, doi:10.2118/101121-MS.
Hansen, K. M., and V. S. Mount (1990), Smoothing and extrapolation of crustal stress orientation measurements, *J. Geophys. Res.*, *95*(B2), 1155–1165, doi:10.1029/JB095iB02p01155.
Heffer, K. J., R. J. Fox, C. A. McGill, and N. C. Koutsabeloulis (1997), Novel techniques show links between reservoir flow directionality, Earth stress, fault structure and geomechanical changes in mature waterfloods, *SPE J.*, *2*(02), 91–98, doi:10.2118/30711-PA.
Heidbach, O., M. Tingay, A. Barth, J. Reinecker, D. Kurfeß, and B. Müller (2008), The World Stress Map database release 2008, doi:10.1594/GFZ.WSM.Rel2008.
Heidbach, O., M. Tingay, A. Barth, J. Reinecker, D. Kurfeß, and B. Müller (2010), Global crustal stress pattern based on the World Stress Map database release 2008, *Tectonophysics*, *482*(1–4), 3–15, doi:10.1016/j.tecto.2009.07.023.
Hill, K. C., N. Hoffman, G. Channon, S. Courteney, R. D. Kendrick, and J. T. Keetlei (2004), Structural styles and hydrocarbon traps in the onshore Taranaki Fold Belt, New Zealand, paper presented at PESA's Eastern Australasian Basin Symposium II, Petroleum Exploration Society of Australia, Adelaide, Australia, 19-22 September.
Hillis, R. R., and S. D. Reynolds (2000), The Australian stress map, *J. Geol. Soc.*, *157*(5), 915–921, doi:10.1144/jgs.157.5.915.
Holt, W. E., and T. A. Stern (1994), Subduction, platform subsidence, and foreland thrust loading: The late Tertiary development of Taranaki Basin, New Zealand, *Tectonics*, *13*(5), 1068–1092, doi:10.1029/94TC00454.
Jaeger, J. C., N. G. W. Cook, and R. Zimmerman (2007), *Fundamentals of Rock Mechanics*, 4th ed., Wiley-Blackwell, Oxford.
King, P. R., and G. P. Thrasher (1996), Cretaceous-Cenozoic geology and petroleum systems of the Taranaki Basin, New Zealand, *Institute of Geological and Nuclear Sciences monograph 13*, 243 p, 246 enclosures, Lower Hutt, New Zealand: Institute of Geological & Nuclear Sciences Limited.
Lallemand, S., A. Heuret, and D. Boutelier (2005), On the relationships between slab dip, back-arc stress, upper plate absolute motion, and crustal nature in subduction zones, *Geochem. Geophys. Geosyst.*, *6*, Q09006, doi:10.1029/2005GC000917.
Lamarche, G., J.-N. Proust, and S. D. Nodder (2005), Long-term slip rates and fault interactions under low contractional strain, Wanganui Basin, New Zealand, *Tectonics*, *24*, TC4004, doi:10.1029/2004TC001699.
Leitner, B., D. Eberhart-Phillips, H. Anderson, and J. L. Nabelek (2001), A focused look at the Alpine fault, New Zealand: Seismicity, focal mechanisms, and stress observations, *J. Geophys. Res.*, *106*(B2), 2193–2220, doi:10.1029/2000JB900303.
Litchfield, N. J., et al. (2013), A model of active faulting in New Zealand, *New Zeal. J. Geol. Geop.*, *57*(1), 32–56, doi:10.1080/00288306.2013.854256.
Lithgow-Bertelloni, C., and J. H. Guynn (2004), Origin of the lithospheric stress field, *J. Geophys. Res.*, *109*(B1), B01408, doi:10.1029/2003JB002467.
Lund, B., and J. Townend (2007), Calculating horizontal stress orientations with full or partial knowledge of the tectonic stress tensor, *Geophys. J. Int.*, *170*(3), 1328–1335, doi:10.1111/j.1365-246X.2007.03468.x.
Mardia, K. V. (1972), *Statistics of Directional Data/K.V. Mardia*, Academic Press, London.
Maxwell, S. C., U. Zimmer, R. W. Gusek, and D. J. Quirk (2009), Evidence of a horizontal hydraulic fracture from stress rotations across a thrust fault, *SPE Prod. Oper.*, *24*(2), 312–319, doi:10.2118/110696-PA.
McKenzie, D. P. (1969), The relation between fault plane solutions for earthquakes and the directions of the principal stresses, *B. Seismol. Soc. Am.*, *59*(2), 591–601.
McNamara, D. D., C. Massiot, B. Lewis, and I. C. Wallis (2015), Heterogeneity of structure and stress in the Rotokawa Geothermal Field, New Zealand, *J. Geophys. Res.: Solid Earth*, *120*, 1243–1262, doi:10.1002/2014JB011480.
Meijer, P. T., and M. J. R. Wortel (1997), Present-day dynamics of the Aegean region: A model analysis of the horizontal pattern of stress and deformation, *Tectonics*, *16*(6), 879–895, doi:10.1029/97TC02004.
Michael, A. J. (1984), Determination of stress from slip data: Faults and folds, *J. Geophys. Res.*, *89*(B13), 11,517–11,526, doi:10.1029/JB089iB13p11517.
Mildren, S. (2009), Mangatoa wellbore stability and fracture susceptibility assessment, *Ministry of Business, Innovation & Employment* (*MBIE*), *New Zealand Unpublished Petroleum Report PR4011*, 68.
Mildren, S., and J. Meyer (2006), Moana prospect cross-fault pressure difference analysis. Northern Taranaki Graben, New Zealand, *Ministry of Economic Development New Zealand Unpublished Petroleum Report PR3647*, 14.
Mildren, S., J. Meyer, and R. Hillis (2001), Pohokura ERD wellbore stability study, *Ministry of Economic Development New Zealand Unpublished Petroleum Reports PR2651*, 70.
Muir, R. J., J. D. Bradshaw, S. D. Weaver, and M. G. Laird (2000), The influence of basement structure on the evolution of the Taranaki Basin, New Zealand, *J. Geol. Soc.*, *157*(6), 1179–1185, doi:10.1144/jgs.157.6.1179.

Müller, B., V. Wehrle, S. Hettel, B. Sperner, and K. Fuchs (2003), A new method for smoothing orientated data and its application to stress data, *Geol. Soc. London, Spec. Pub.*, *209*(1), 107–126, doi:10.1144/gsl.sp.2003.209.01.11.

Nairn, I. A., and J. W. Cole (1981), Basalt dikes in the 1886 Tarawera Rift, *New Zeal J Geol Geop*, *24*(5-6), 585–592, doi:10.1080/00288306.1981.10421534.

Neall, V. E., R. B. Stewart, and I. E. M. Smith (1986), History and petrology of the Taranaki Volcanoes. Late Cenozoic volcanism in New Zealand, *R. Soc. N. Z. Bull.*, *23*, 251–264.

Nicol, A., and J. Beavan (2003), Shortening of an overriding plate and its implications for slip on a subduction thrust, central Hikurangi Margin, New Zealand, *Tectonics*, *22*(6), 1070, doi:10.1029/2003TC001521.

Nicol, A., C. Mazengarb, F. Chanier, G. Rait, C. Uruski, and L. Wallace (2007), Tectonic evolution of the active Hikurangi subduction margin, New Zealand, since the Oligocene, *Tectonics*, *26*, TC4002, doi:10.1029/2006TC002090.

Nicol, A., V. Stagpoole, and G. Maslen (2004), Structure and petroleum potential of the Taranaki fault play, in *2004 New Zealand Petroleum Conference*, edited, p., Wellington, Crown Minerals, Ministry of Economic Development, pp. 9.

Nicol, A., and L. M. Wallace (2007), Temporal stability of deformation rates: Comparison of geological and geodetic observations, Hikurangi subduction margin, New Zealand, *Earth Planet. Sci. Lett.*, *258*(3–4), 397–413, doi:10.1016/j.epsl.2007.03.039.

Nicol, A., J. Walsh, K. Berryman, and S. Nodder (2005), Growth of a normal fault by the accumulation of slip over millions of years, *J. Struct. Geol.*, *27*(2), 327–342.

Palmer, J., and G. Bulte (1991), Taranaki Basin, New Zealand, in *Active Margin Basins—AAPG Memoir*, edited by K. Biddle, pp. 262–282, AAPG, Tulsa, Okla.

Pierdominici, S., and O. Heidbach (2012), Stress field of Italy—Mean stress orientation at different depths and wave-length of the stress pattern, *Tectonophysics*, *532–535*(0), 301–311, doi:10.1016/j.tecto.2012.02.018.

Plumb, R. A., and S. H. Hickman (1985), Stress-induced borehole elongation: A comparison between the four-arm dipmeter and the borehole televiewer in the Auburn Geothermal Well, *J. Geophys. Res.*, *90*(B7), 5513–5521, doi:10.1029/JB090iB07p05513.

Rajabi, M., S. Sherkati, B. Bohloli, and M. Tingay (2010), Subsurface fracture analysis and determination of in-situ stress direction using FMI logs: An example from the Santonian carbonates (Ilam Formation) in the Abadan Plain, Iran, *Tectonophysics*, *492*(1–4), 192–200, doi:10.1016/j.tecto.2010.06.014.

Rajabi, M., M. Tingay, and O. Heidbach (2014), The present-day stress pattern in the Middle East and Northern Africa and their importance: The World Stress Map database contains the lowest wellbore information in these petroliferous areas, in *International Petroleum Technology Conference*, edited, International Petroleum Technology Conference, Doha, Qatar, doi:10.2523/IPTC-17663-MS.

Rajabi, M., M. Tingay, and O. Heidbach (2016a), The present-day stress field of New South Wales, Australia, *Aust. J. Earth Sci.*, *63*(1), 1–21, doi:10.1080/08120099.2016.1135821.

Rajabi, M., M. Tingay, R. King, and O. Heidbach (2016b), Present-day stress orientation in the Clarence-Moreton Basin of New South Wales, Australia: A new high density dataset reveals local stress rotations, *Basin Res.*, doi:10.1111/bre.12175.

Raleigh, C. B., J. H. Healy, and J. D. Bredehoeft (1972), Faulting and crustal stress at Rangely, Colorado, in *Flow and Fracture of Rocks*, edited by H. C. Heard et al., pp. 275–284, U.S. Geological Survey, Washington, D. C., doi:10.1029/GM016p0275.

Reilly, C., A. Nicol, J. J. Walsh, and H. Seebeck (2015), Evolution of faulting and plate boundary deformation in the southern Taranaki Basin, New Zealand, *Tectonophysics*, *651–652*(0), 1–18, doi:10.1016/j.tecto.2015.02.009.

Reinecker, J., M. Tingay, and B. Müller (2003), Borehole breakout analysis from four-arm caliper logs. [Available at http://dc-app3-14.gfz-potsdam.de/pub/guidelines/WSM_analysis_guideline_breakout_caliper.pdf.]

Reiter, K., O. Heidbach, D. Schmitt, K. Haug, M. Ziegler, and I. Moeck (2014), A revised crustal stress orientation database for Canada, *Tectonophysics*, *636*, 111–124, doi:10.1016/j.tecto.2014.08.006.

Reyners, M. (1980), A microearthquake study of the plate boundary, North Island, New Zealand, *Geophys. J. Roy. Ast.r S.*, *63*(1), 1–22, doi:10.1111/j.1365-246X.1980.tb02607.x.

Reyners, M. (2010), Stress and strain from earthquakes at the southern termination of the Taupo Volcanic Zone, New Zealand, *J. Volcanol. Geotherm. Res.*, *190*(1–2), 82–88, doi:10.1016/j.jvolgeores.2009.02.016.

Richardson, R. M. (1992), Ridge forces, absolute plate motions, and the intraplate stress field, *J. Geophys. Res.*, *97*(B8), 11,739–11,748, doi:10.1029/91JB00475.

Robinson, R., I. M. Calhaem, and A. A. Thomson (1976), The Opunake, New Zealand, earthquake of 5 November 1974, *N. Z. J. Geol. Geop.*, *19*(3), 335–345, doi:10.1080/00288306.1976.10423563.

Salazar, M., L. Moscardelli, and L. Wood (2015), Utilising clinoform architecture to understand the drivers of basin margin evolution: A case study in the Taranaki Basin, New Zealand, *Basin Res.*, doi:10.1111/bre.12138.

Salmon, M., B. L. N. Kennett, T. Stern, and A. R. A. Aitken (2013), The Moho in Australia and New Zealand, *Tectonophysics*, *609*(0), 288–298, doi:10.1016/j.tecto.2012.07.009.

Sbar, M. L., M. Barazangi, J. Dorman, C. H. Scholz, and R. B. Smith (1972), Tectonics of the Intermountain Seismic Belt, Western United States: Microearthquake seismicity and composite fault plane solutions, *GSA Bull.*, *83*(1), 13–28.

Sbar, M. L., and L. R. Sykes (1973), Contemporary compressive stress and seismicity in eastern North America: An example of intra-plate tectonics, *Geol. Soc. Am. Bull.*, *84*(6), 1861–1882, doi:10.1130/0016-7606(1973)84<1861:ccsasi>2.0.co;2.

Seebeck, H., A. Nicol, M. Giba, J. Pettinga, and J. Walsh (2013), Geometry of the subducting Pacific plate since 20 Ma, Hikurangi margin, New Zealand, *J. Geol. Soc.*, doi:10.1144/jgs2012-145.

Seebeck, H., A. Nicol, P. Villamor, J. Ristau, and J. Pettinga (2014), Structure and kinematics of the Taupo Rift, New Zealand, *Tectonics*, *33*(6), 1178–1199, doi:10.1002/2014TC003569.

Sherburn, S., and R. S. White (2005), Crustal seismicity in Taranaki, New Zealand using accurate hypocentres from a dense network, *Geophys. J. Int.*, *162*(2), 494–506, doi:10.1111/j.1365-246X.2005.02667.x.

Sherburn, S., and R. S. White (2006), Tectonics of the Taranaki region, New Zealand: Earthquake focal mechanisms and stress axes, *N. Z. J. Geol. Geop.*, *49*(2), 269–279, doi:10.1080/00288306.2006.9515165.

Sibson, R. H. (1985), Stopping of earthquake ruptures at dilational fault jogs, *Nature*, *316*(6025), 248–251.

Sibson, R. H. (1996), Structural permeability of fluid-driven fault-fracture meshes, *J. Struct. Geol.*, *18*(8), 1031–1042.

Sibson, R. H., F. C. Ghisetti, and R. A. Crookbain (2012), Andersonian wrench faulting in a regional stress field during the 2010–2011 Canterbury, New Zealand, earthquake sequence, *Geol. Soc. London Spec. Publ.*, *367*(1), 7–18, doi:10.1144/sp367.2.

Sperner, B., B. Müller, O. Heidbach, D. Delvaux, J. Reinecker, and K. Fuchs (2003), Tectonic stress in the Earth's crust: Advances in the World Stress Map project, *Geol. Soc. London Spec. Publ.*, *212*(1), 101–116, doi:10.1144/gsl.sp.2003.212.01.07.

Spinks, K. D., V. Acocella, J. W. Cole, and K. N. Bassett (2005), Structural control of volcanism and caldera development in the transtensional Taupo Volcanic Zone, New Zealand, *J. Volcanol. Geotherm. Res.*, *144*(1–4), 7–22, doi:10.1016/j.jvolgeores.2004.11.014.

Stagpoole, V., and R. Funnell (2001), Arc magmatism and hydrocarbon generation in the northern Taranaki Basin, New Zealand, *Pet. Geosci.*, *7*(3), 255–267, doi:10.1144/petgeo.7.3.255.

Stagpoole, V., R. Funnell, and A. Nicol (2004), Overview of the structure and associated petroleum prospectivity of the Taranaki fault, New Zealand, in *PESA's Eastern Australian Basins Symposium II*, edited by P. J. Boult, D. R. Johns, and S. C. Lang, pp. 197–206, Petroleum Exploration Society of Australia, Adelaide, South Australia.

Stern, T., G. Houseman, M. Salmon, and L. Evans (2013), Instability of a lithospheric step beneath western North Island, New Zealand, *Geology*, *41*(4), 423–426.

Stern, T. A., and F. J. Davey (1990), Deep seismic expression of a foreland basin: Taranaki basin, New Zealand, *Geology*, *18*(10), 979–982, doi:10.1130/0091-7613(1990)018<0979:dseoaf>2.3.co;2.

Tingay, M., C. Morley, R. King, R. R. Hillis, D. D. Coblentz, and R. Hall (2010), Present-day stress field of Southeast Asia, *Tectonophysics*, *482*(1–4), 92–104, doi:10.1016/j.tecto.2009.06.019.

Tingay, M., B. Müller, J. Reinecker, O. Heidbach, F. Wenzel, and P. Fleckenstein (2005), Understanding tectonic stress in the oil patch: The World Stress Map Project, *Leading Edge*, *24*(12), 1276–1282, doi:10.1190/1.2149653.

Tingay, M. R. P., M. L. Rudolph, M. Manga, R. J. Davies, and C.-Y. Wang (2015), Initiation of the Lusi mudflow disaster, *Nat. Geosci.*, *8*(7), 493–494, doi:10.1038/ngeo2472.

Townend, J., S. Sherburn, R. Arnold, C. Boese, and L. Woods (2012), Three-dimensional variations in present-day tectonic stress along the Australia–Pacific plate boundary in New Zealand, *Earth Planet. Sci. Lett.*, *353–354*(0), 47–59, doi:10.1016/j.epsl.2012.08.003.

Townsend, D., et al. (2010), Palaeoearthquake histories across a normal fault system in the southwest Taranaki Peninsula, New Zealand, *N. Z. J. Geol. Geop.*, *53*(4), 375–394, doi:10.1080/00288306.2010.526547.

Walcott, R. I. (1987), Geodetic strain and the deformation history of the North Island of New Zealand during the late Cainozoic, *Philos. Trans. R. Soc. London Ser. A*, *321*, 163–181.

Wallace, L. M., J. Beavan, R. McCaffrey, and D. Darby (2004), Subduction zone coupling and tectonic block rotations in the North Island, New Zealand, *J. Geophys. Res.*, *109*, B12406, doi:10.1029/2004JB003241.

Wallace, L. M., S. Ellis, and P. Mann (2009), Collisional model for rapid fore-arc block rotations, arc curvature, and episodic back-arc rifting in subduction settings, *Geochem. Geophys. Geosyst.*, *10*, Q05001, doi:10.1029/2008GC002220.

Wang, K. (2000), Stress–strain 'paradox', plate coupling, and forearc seismicity at the Cascadia and Nankai subduction zones, *Tectonophysics*, *319*(4), 321–338, doi:10.1016/S0040-1951(99)00301-7.

Webb, T. H., and H. Anderson (1998), Focal mechanisms of large earthquakes in the North Island of New Zealand: Slip partitioning at an oblique active margin, *Geophys. J. Int.*, *134*(1), 40–86, doi:10.1046/j.1365-246x.1998.00531.x.

Webb, T. H., B. G. Ferris, and J. S. Harris (1986), The Lake Taupo, New Zealand, earthquake swarms of 1983, *N. Z. J. Geol. Geop.*, *29*(4), 377–389, doi:10.1080/00288306.1986.10422160.

Webster, M., S. O'Connor, B. Pindar, and R. Swarbrick (2011), Overpressures in the Taranaki Basin: Distribution, causes, and implications for exploration, *AAPG Bull.*, *95*(3), 339–370, doi:10.1306/06301009149.

Ziegler, M., M. Rajabi, O. Heidbach, G. P. Hersir, K. Ágústsson, S. Árnadóttir, and A. Zang (2016), The stress pattern of Iceland, *Tectonophysics*, *674*, 101–113, doi:10.1016/j.tecto.2016.02.008.

Zoback, M. D. (2007), *Reservoir Geomechanics*, pp. 464, Stanford University, California.

Zoback, M. L. (1992), First- and second-order patterns of stress in the lithosphere: The World Stress Map Project, *J. Geophys. Res.*, *97*(B8), 11,703–11,728, doi:10.1029/92JB00132.

Zoback, M. L., and M. D. Zoback (1980), Faulting patterns in north-central Nevada and strength of the crust, *J. Geophys. Res.*, *85*(B1), 275–284, doi:10.1029/JB085iB01p00275.

Zoback, M. L., et al. (1989), Global patterns of tectonic stress, *Nature*, *341*(6240), 291–298.